Energy evaluation and treatment efficiency of vacuum membrane distillation for brackish water desalination

Mohammad Ramezanianpour and Muttucumaru Sivakumar

ABSTRACT

Strict environmental regulations have led to the rapid development of membrane separation technologies for the production of potable water, for industrial water supply, and for the reuse and discharge of treated wastewater. Promotion of water recycling and the provision of potable water from brackish water prevent significant negative effects on the environment and drinking water supplies. This study is intended to describe and compare a sustainable technology for brackish water treatment. Among the four configurations of the membrane distillation process, vacuum membrane distillation (VMD) produces higher flux and results in a low fouling rate. It comprises evaporation and condensation that mimics what occurs in nature. Mathematical models proposed for the VMD transport mechanisms are incorporated to predict the actual experimental flux. The response of the flux rate to various process operating parameters is demonstrated. Variation of effective parameters is investigated in terms of energy consumption. The data indicate that the permeate flux is highly responsive to the variation of pressure and temperature. VMD enables the removal of 99.9% of total dissolved solids from natural and contaminated water sources. The findings are that the quality of the permeate water from all sources was at acceptable standards for potable use.

Key words | brackish water, desalination, heat and mass transfer, mathematical modeling, specific energy consumption, vacuum membrane distillation

Mohammad Ramezanianpour
Muttucumaru Sivakumar (corresponding author)
Faculty of Engineering and Information Sciences,
GeoQuest Research Centre, School of Civil,
Mining and Environmental Engineering,
University of Wollongong,
New South Wales 2522,
Australia
E-mail: *siva@uow.edu.au*

INTRODUCTION

Treatment of brackish water from vital water supply sources is a common approach for fresh water production. In many countries, alternative sources of fresh water are groundwater and seawater. The quality and quantity of groundwater is equally important for a number of reasons. Most groundwater aquifers are subjected to severe stress due to excess pumping and this affects groundwater and surface water levels. The groundwater quality can deteriorate due to contamination from various diffused and point sources and this poses a serious concern. The physical and chemical water quality variation of groundwater is a function of geological formations and anthropogenic activities. Groundwater quality is greatly influenced by mineral ions from soil particles and sediment. Dissolved solids originating in the precipitated water are divided into three categories. Total dissolved solids (TDS) include major elements such as Na, Ca, Mg, HCO_3, SO_4, and Cl which comprise 1–1,000 mg/L TDS and Fe, K, CO_2, F, and NO_3 which comprise 0.01–10 mg/L. Finally, trace components contribute the small amount of 0.0001–0.1 mg/L TDS. Seawater is a vast available resource for coastal cities, however, in some cases, a variety of land-based pollutants from industrial, domestic, and agricultural areas results in contamination of coastal waters. Seawater TDS content may vary from 7,000 mg/L in the Baltic Sea up to 45,000 mg/L in the Persian Gulf. The average concentration of the majority of seawater is 19,700 mg/L of Cl, 10,900 mg/L of Na, 2,740 mg/L of SO_4, 1,310 mg/L of Mg, and 410 mg/L of Ca. Reuse of brackish water such as mine water prevents significant damage to in-stream ecosystems and reduces the consumption of other good quality water sources. Mine drainage quality is influenced by excavation type

doi: 10.2166/wrd.2014.025

(surface mining and sub-surface mining), mine location, the mining process, and the source of the water. Conversely, underground mines require large amounts of water to be pumped from aquifers. The dominant cations and anions observed in mine drainage are Fe, Ca, Mg, CO_3, Cl, and SO_4. Therefore, the necessity to provide fresh water from contaminated water sources continues to receive much attention in the scientific community due to the inequity between supply and demand. The impacts on the environment and human health, and the search for solutions to mitigate these, have become the focus of a number of research initiatives. This is due to reasons such as social acceptance and community perception, health hazards, cost of production, population growth forecasts, and economic development. These interests provide opportunities for membrane distillation (MD) to be studied and developed as one solution to the problems.

MD is a thermally driven separation process, which uses hydrophobic porous membranes to separate a gaseous phase from the entry liquid (Qtaishat *et al.* 2008). A negative pressure, or coolant flow, on the permeate side implies physical separation in all four configurations of MD, i.e., direct contact membrane distillation (DCMD), sweeping gas membrane distillation (SGMD), vacuum membrane distillation (VMD), and air gap membrane distillation (AGMD) (Alkhudhiri *et al.* 2012). In recent years, there has been growing interest in desalination using VMD technology. Overall, 40.3% of the VMD publications up to December 2010 dealt with theoretical models (Khayet & Matsuura 2011). The mechanism of mass and heat transfer in VMD has been critically developed in recent decades (Lawson & Lloyd 1996; Guijt *et al.* 2000; Khayet & Matsuura 2004; Alklaibi & Lior 2005; Al-Obaidani *et al.* 2008; Khayet 2011; Zhang *et al.* 2013), so it is important to investigate the accuracy of the developed models via experimental data. Small scale experimental VMD processes have been designed, constructed, and installed (Xu *et al.* 2006; Criscuoli *et al.* 2008; Sivakumar *et al.* 2013b) in order to monitor the performance of VMD. However, very few papers have focused on the application of VMD in water treatment and the energy efficiency of this technology. VMD produces ultra-pure water as it rejects all non-volatile constituents such as ions, dissolved non-volatile organics, colloids, and pathogenic microorganisms. The VMD technique has a number of advantages over the other conventional MD techniques; perhaps, the most notable of these are the higher flux rate and the lower fouling rate compared to other MD configurations for the same operating conditions. Distilled water can also be produced at lower operating temperatures, resulting in lower operating costs (Safavi & Mohammadi 2009). The liquid–vapor interface minimizes heat transfer losses within the VMD process and increases the rate of permeate flux; therefore, less energy is required to achieve similar flux rates, compared to other MD configurations and pressure-driven desalination processes (Mericqa *et al.* 2011). Safavi & Mohammadi (2009) investigated the energy consumption of a small scale VMD process for seven different configurations of pressure and flow rates at a constant temperature. It has been shown that efficient operation consumes 1.67 kWh/kg of energy to produce 9.6 kg/m^2h of permeate flux. Specific energy has been varied from 1.70 to 3.96 kWh/kg for further operating configurations.

Application of VMD has been limited primarily to the extraction of volatile organic compounds from aqueous solutions and rarely to desalination. Li *et al.* (2003) compared the permeate flux of a DCMD and a VMD process using a synthetic seawater solution. It was concluded that VMD permeated more distillate water than the DCMD process. The study was focused on different membrane applications and the quality and efficiency of the processes. A 5-month experiment with a pilot-scale VMD on a ship was conducted, and salt concentration was reduced to below 3 mg/L from the seawater source (Xu *et al.* 2006). The tests were conducted at a constant temperature of 55 °C and a downstream pressure of 7 kPa. The efficient usage of energy generated by waste-heat was verified for a constant operating condition. Water permeate flux and salt rejection were analyzed via VMD using four different types of coated membranes (Jin *et al.* 2008). The salt rejection of the silicone rubber-coated membrane remained constant at 99% for a short 6-h test; however, it decreased from 99 to 96% in a longer experiment over 14 days. The salt rejection of polytrifluoropropylsiloxane rubber without a forepolymerization-coated membrane decreased from 99 to 95% and from 98 to 88% for short-term and long-term tests, respectively. The flux decay attributed to the formation of salt crystals on the membrane surface was also observed for each set-up. The performance of tubular ceramic membranes Zr50 and Ti5, with pore diameters of

50 and 5 nm, respectively, was evaluated for the desalination of the 0.5 and 1 M NaCl solution (Cerneaux *et al.* 2009). The efficiency of VMD, in terms of the removal rate, was 99 ± 1% in two cases for Ti5, however, rejection rates decreased from 99 to 96% for Zr50. The tests were performed for only 4 h, and the study focused on the comparison of flux and rejection rates with DCMD and AGMD. Different concentrations of NaCl solutions from 15 up to 300 g/L were used in VMD, and no traces of salt were observed in the permeate, despite the very high concentration of the influent (Wirth & Cabassud 2002). No specific value was reported for the rate of salt rejection and the remaining water quality parameters. A high rejection rate for NaCl solution with concentrations of 50–150 g/L was achieved in nine different VMD configurations (Mohammadi & Safavi 2009). TDS of the permeate samples lies between 0.08 and 1.90 ppm. The sensitivity of the flux to the operating parameters was studied, but the effect of these parameters on energy consumption and the quality of the permeate were not illustrated. VMD was used on reverse osmosis (RO) brines with a total concentration of 38.9 g/L, obtained from a plant located on the Mediterranean Sea (Mericq *et al.* 2010). It was shown that the water recovery increased from 40 to 89%, and the brine was 7.6 times more concentrated. It was also observed that the permeate flux is rarely sensitive to temperature and concentration polarization even for the high salt concentrations. The impact of membrane surface scaling on the decline rate of permeate flux was shown to be very limited. The effect of three different synthetic solutions with conductivity of 77.8, 106.4, and 149.3 mS/cm on the membrane fouling was monitored and the scaling components were determined. Although the concentration of the major ions were measured in the feed solution, the quality of the permeate water was not discussed. What is missing from all of the above-mentioned research is an evaluation of the efficiency of VMD in terms of the permeate water quality and specific energy consumption in the desalination of seawater or the treatment of brackish or wastewater.

THEORETICAL BACKGROUND

Membrane characteristics play an important role in the rate of permeate flux. The hydrophobicity of the membrane, porosity, surface area in contact with feed solution, thermal stability of materials, pore size distribution, membrane thickness, and liquid entry pressure are all factors affecting VMD performance. A higher flux rate can be achieved by higher porosity, larger pore size, and suitable coating of the membranes. However, larger pore radius (r) reduces the critical entry pressure required for feed water to infiltrate the membrane pores. The pressure difference across the membrane (ΔP) is influenced directly by the surface tension of the feed solution and the cosine of the contact angle (φ) between the feed solution and the membrane surface. A decline of surface tension (γ) and contact angle will decrease ΔP, as shown in Equation (1). Conversely, the pore size must be small enough to prevent the penetration of the liquid feed and large enough to facilitate high mass transfer. Therefore, the ideal pore size is influenced by the membrane material and the characteristics of feed solution.

$$\Delta P = \frac{2\gamma\cos\varphi}{r} \tag{1}$$

The concept of vapor flux and heat transfer through a hydrophobic membrane in VMD is illustrated in Figure 1. The feed-solution temperature (T_f) is decreased across the bulk media to the membrane feed-side temperature (T_{fm}) and the permeate-side temperature of the membrane (T_{pm}) is also decreased to the vapor temperature (T_p). The feed solution is passed on one side of the membrane and treated by a thermally driven separation process. Water molecules in a gaseous vapor state are transported through the microporous

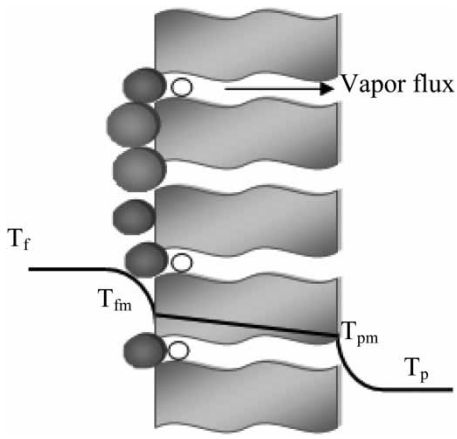

Figure 1 | Mass transfer and heat transfer through the membrane in VMD.

membrane. Mass transfer in VMD is accomplished by applying vacuum pressure at the permeate side of the membrane.

The heat and mass transfer mechanisms in VMD are described by the kinetic theory of gasses. A model or a combination of the Knudsen flow and the viscous flow explains mass transfer in VMD. The ratio of the mean free path of the transported vapor molecules, λ, to the diameter of the membrane pores, d, i.e., the Knudsen number ($K_n = \lambda/d$), provides a guideline to determine the most accurate mechanism of mass transfer for the given operating conditions. For a given diameter, the Knudsen number is obtained using the estimation of mean free path through Equation (2) (Lawson & Lloyd 1997)

$$\lambda = \frac{k_B T}{\sqrt{2}\pi P \sigma^2} \tag{2}$$

where k_B is the Boltzmann constant (1.381×10^{-23} J/K), T is the absolute temperature, P is the mean pressure within the membrane pores and σ is the collision diameter (2.641 Å for water vapor). For a membrane with small pores ($K_n > 1$), molecule–pore wall collisions are more frequent. The Knudsen diffusion model expressed in Equation (3) assumes a Knudsen flow regime for vapor passing through small holes in a thin wall (Lawson & Lloyd 1997; Khayet *et al.* 2004). The number of molecules passing through a pore is directly proportional to the driving pressure of the gas and inversely proportional to its molecular weight.

$$N_w = \frac{K\Delta P}{R\delta T_{fm}} \left(\frac{8RT}{\pi M_w}\right)^{\frac{1}{2}} \tag{3}$$

where N_w is the molar flux (mol/m^2.s), ΔP (Pa) is the pressure difference between the partial pressure of the solution and the absolute vacuum pressure, R is the gas constant (8.31 J/mol.K), δ is the membrane thickness (m), T_{fm} indicates temperature at the feed side of the membrane surface, M_w is the molecular weight of water (18.01528 g/mol) and K, the Knudsen diffusion constant (m) can be expressed by Equation (4) as follows:

$$K = \frac{2\epsilon r}{3\tau} \tag{4}$$

where ϵ is the membrane porosity, r is the average of the pores radius (m), and τ is the membrane tortuosity, which is the ratio of the pore thickness to the actual molecular flow path through the pore. By determining the vapor temperature at the feed side of the membrane, the vapor flow rate is estimated using a value for the molar flux rate. The mass flow rate, $\dot{m}_v$ (kg/s) of vapor through membrane pores is calculated using Equation (5).

$$\dot{m}_v = N_w A_m M_w \tag{5}$$

where A_m is the total membrane surface area (m^2). The vapor temperature at the feed side of the membrane is derived using Equation (6) (Qtaishat *et al.* 2008).

$$T_{fm} = T_f - \frac{\dot{m}_v H_v}{h_f A_m} \tag{6}$$

where the latent heat of vaporization of the water, H_v (J/kg), is determined from standard tables for different water temperatures. The feed-water velocity, u_f (m/s), affects the degree of heat loss between the feed water and the feed side of the membrane surface. The heat transfer coefficient of the feed solution h_f (W/m^2.K) depends on the Nusselt number (Nu), which is proportional to the Reynolds number and Prandtl number. The feed-water heat transfer coefficient is derived using Equation (7).

$$h_f = \frac{Nuk_T}{2r} \tag{7}$$

where k_T is the thermal conductivity of the feed solution (W/m.K).

Pressure difference across the membrane determines the permeate flux rate when multiplied by the permeability of the membrane. Saturation pressure of the feed solution at the feed side of the membrane and vacuum pressure applied on the permeate side create this difference. Saturation pressure is related to the feed-side temperature. The well-known Antoine's equation expressed in Equation (8) relates temperature to the water vapor saturation pressure $P_{sat}(T_{fm})$ at the liquid–vapor interface (Mengual *et al.* 2004).

$$P_{sat}(T_{fm}) = e^{\left(23.1964 - \frac{3816.44}{-46.13 + T_{fm}}\right)} \tag{8}$$

The curvature of the liquid–vapor surface is assumed to have negligible effect in this equation. The saturation pressure is modified by the TDS concentration of the feed solution. Partial pressure, p_w (Pa) is expressed by Equation (9),

$$p_w = x_w a_w P_{sat}(T_{fm}) \tag{9}$$

where x_w is the water mole fraction derived from the concentration of salts in water and a_w is the activity coefficient of water, which is derived by Equation (10) (Lawson & Lloyd 1997).

$$a_w = 1 - 0.5x_{NaCl} - 10x_{NaCl}^2 \tag{10}$$

where x_{NaCl} is the sodium chloride (NaCl) mole fraction.

Viscous flow rises for a membrane with large pores ($K_n < 0.01$), so that the molecule–molecule collision is dominant. In this case, Equation (11) was proposed to determine the total flux (Lawson & Lloyd 1997; Khayet & Matsuura 2004).

$$N_w = \frac{\pi r^4 P_{ave}}{8\mu R T_{fm} A_m \tau \delta}\Delta P \tag{11}$$

where P_{ave} is average partial pressure (Pa) and μ is dynamic viscosity (Pa.s).

In the transition region ($0.01 < K_n < 1$), both molecule–molecule and molecule–pore wall collisions have to be considered. In addition, surface diffusion is negligible for membranes with a pore size $>0.02\,\mu m$ due to the fact that pore area is significantly larger than the surface-diffusion area. The Dusty-Gas model was developed in the transition region to describe VMD performance (Guijt *et al.* 2000). Equation (12) is based on the assumption of both molecule–pore wall and molecule–molecule interactions.

$$N_w = \frac{\Delta P}{RT_{fm}}\left[Kv_m + B\frac{P_{ave}}{\mu}\right]\frac{1}{R_{out}\ln\left(\frac{R_{out}}{R_{in}}\right)} \tag{12}$$

where R_{out} and R_{in} are outer and inner radius of the hollow fiber (m), respectively, v_m is mean molar gas velocity (m/s), and B is the viscous flow morphology parameter (m^2) derived by Equation (13).

$$B = \frac{\varepsilon r^2}{8\tau} \tag{13}$$

The Knudsen–viscous type of diffusion in the transition region for describing mass transfer through a porous membrane in VMD was proposed as Equation (14) (Khayet 2011).

$$N_w = \frac{\Delta P}{\delta R T_{fm}}\left[K\left(\frac{8RT_{fm}}{\pi M_w}\right)^{\frac{1}{2}} + B\frac{P_{ave}}{\mu}\right] \tag{14}$$

A new model presented in Equation (15) has also been recently developed for the Knudsen–viscous flow diffusion transition mechanism. The model combines viscous flow and Knudsen diffusion (Zhang *et al.* 2013).

$$N_w = \left[\frac{8}{3}\frac{r\varepsilon}{b\tau}\left(\frac{1}{2\pi M_w R T_{fm}}\right)^{\frac{1}{2}} + \frac{1}{8\mu}\frac{\varepsilon r^2}{b\tau}\frac{P_{ave}}{RT_{fm}}\right]\Delta P \tag{15}$$

where b is the thickness of the membrane ($b = R_{in}\ln(R_{out}/R_{in})$).

The main difference in the models presented in Equations (12), (14), and (15) is the definition of the membrane thickness. It is specified as a simple thickness of the membrane given by the manufacturer or the log form of inner and outer diameters. In addition, Equation (15) considered the effect of Knudsen diffusion to be two times higher than the other two equations. At higher temperatures, the variation is noticeable. The models presented predict flux response to changes in temperature, pressure, flow rate, and feed-solution characteristics for a specific membrane. In this research, the Knudsen number has been calculated to be in the range of 0.01–1, hence the most important phenomenon in mass transfer is Knudsen–viscous flow. The models presented are employed to predict the flux variation over a variety of experimental conditions.

EXPERIMENTS

The experimental arrangement of VMD using a commercial tubular membrane at a laboratory scale is shown in Figure 2.

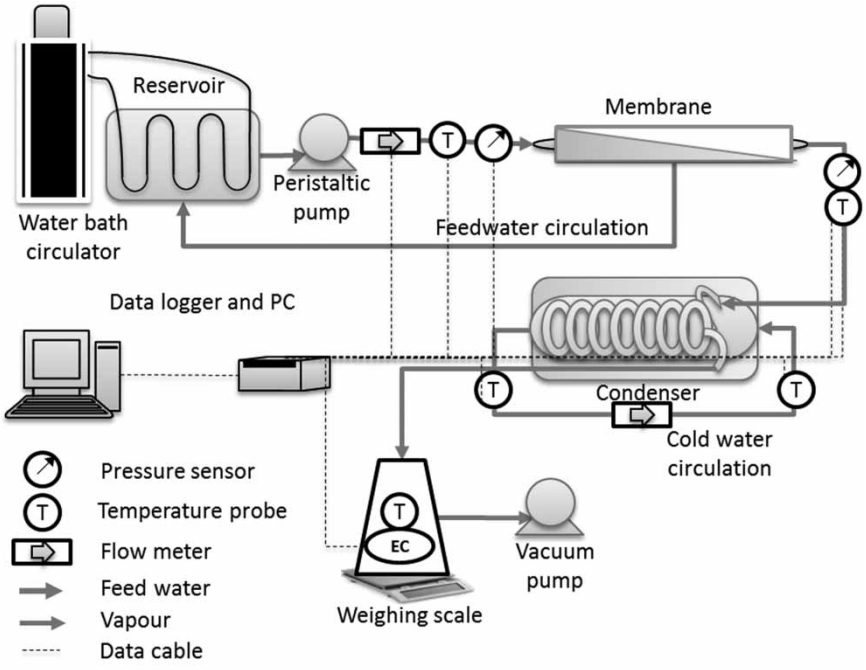

Figure 2 | VMD experimental set-up.

The experiments were conducted by monitoring the effects of various operating parameters such as pressure, temperature, flow rate, and salinity on vapor flux. Feed water was warmed in an insulated reservoir by a temperature-controlled water bath circulator. The digitally controlled water bath supplied the pre-determined heat to the feed water, adjusting the temperature at the membrane inlet. A Masterflex peristaltic pump circulated the feed-water solution through the membrane module. The effects of the flow rate were monitored, incorporating a flow meter mounted on the feed-water pump. The recirculation hose was kept above the membrane level, keeping the membrane module full at all times. Membranes used in VMD need to be significantly more hydrophobic than other MD processes due to the existence of vacuum pressure. This favors wetting of the membrane pores and liquid penetration. In this study, a hollow fiber polypropylene (PP) membrane module, MD02CP2N (MICRODYN), with 40 capillaries was used. The surface area and pore diameter, as indicated by the manufacturer, are 0.1 m^2 and 0.2 μm, respectively. The vacuum pressure on the permeate side of the membrane was applied when the temperature reached a higher value than the saturation temperature. A ball valve was fitted into a N820 Javac KNF laboratory vacuum pump to control the vacuum pressure on the permeate side. This was precisely monitored by a pressure gauge. The pump creates vacuum pressure through the condensation column at the permeate side of the membrane. A condensation column was placed across the vacuum pump and the permeate side of the membrane to condense vapor into a liquid phase. Water vapor was passed through a glass condensation column containing three cavities. These cavities are a spiral tube connected to the vacuum pump, a cold water cylinder, and a condensed vapor tunnel, as shown in Figure 2.

Commercial and industrial applications of VMD were assessed by the desalination of the feed saline solution made by NaCl and various saline water sources, which were collected for analysis purposes. Groundwater samples were taken from the Wagon Wheels farm, located in Stanwell Tops, NSW and the PRB site well no. 27. Seawater was collected from Wollongong harbor, and mine water samples were gathered from the BHP Billiton-owned Westcliff mine site located in Appin, NSW and the Gujarat NRE coal mine located in Bellambi, NSW. Swimming pool salt-water samples from the University of Wollongong's

swimming pool were also collected due to its high level of dissolved salts and the potential for microbial contamination. A high chlorine level is necessary for the sanitizing of salt water and the chlorine might be present in the form of hypochlorous acid. Nitrogenous compounds derived from urine and sweat, and disinfection byproducts such as chloroform and chloroacetic acids, also often form in swimming pool water. For this reason, the efficiency of VMD in the treatment of a salt-water sample from the swimming pool was assessed. Sodium chloride was mixed with distilled water to obtain different concentrations of saline solution to study the effect of salinity on permeate flux. The contribution of each parameter to the flux rate increment was determined. Energy efficiency was evaluated by measuring specific energy consumption for each set of experimental conditions. The energy consumption of the vacuum pump, the circulation pump, and the water bath circulator was monitored using a power meter for each test. Finally, the treatment efficiency of the VMD process was determined by measuring and comparing the quality of the raw and the desalinated brackish water samples. Water quality parameters such as TDS, pH, total coliforms, total organic carbon (TOC), and total nitrogen (TN) and the concentration of Na, Ca, Mg, and Fe were analyzed for each sample before and after the treatment process.

DISCUSSION OF RESULTS

Mass transfer

The effect of vacuum pressure was investigated by decreasing the absolute pressure of the permeate side from 20 to 7 kPa and running the system at various vacuum intervals within this range while all other parameters remained constant. Feed-water temperatures from 45 to 65 °C were selected in steps of 5 °C, as temperature above the maximum value was considered not only as detrimental to the membranes, but also as requiring more energy for heating. Conversely, high vacuum pressure is necessary to evaporate feed water at low temperatures, which also results in higher energy consumption. Feed-water flow rate increased from 0.5 to 6.90 L/min while other variable parameters were kept constant to monitor the variation of the permeate flux.

The results of the flux variation with vacuum pressure, feed-water temperature, and flow rate are illustrated in Figure 3. Flow rate variation is depicted in five graphs. In each graph, four series of experimental and modeled flux are presented for each absolute pressure on the permeate side. The Knudsen–viscous diffusion models were applied to replicate the trend of flux versus temperature rise. Vacuum pressure was observed to change non-monotonically, and this had the most significant effect on flux among the variables studied. It was found that an increase in pressure on the permeate side of the membrane results in a severe decrease in the permeate flux rate due to a significant reduction in the driving force of the transmembrane flux. These results are consistent with many of the findings in the literature (Banat *et al.* 2003; Safavi & Mohammadi 2009; Chen *et al.* 2011). Feed-water temperature had a considerable effect on vapor permeation flux. For a given set of experimental conditions, the permeate flux was raised exponentially as feed-water temperature increased. This can be attributed to the fact that an increase in temperature raises the water vapor pressure, which is the main driving force for water vaporization (Al-Asheh *et al.* 2006). Temperature also increases the Reynolds number, which, in turn, raises the heat transfer coefficient followed by temperature at the feed side of the membrane, eventually increasing the flux. The Knudsen–viscous diffusion model (Equation (14)) predicts reasonably well the experimental flux data in various situations. It can be seen from Figure 3 that, for this particular type of membrane, the models predicted conflicting results at higher temperatures. Conversely, optimized feed-water temperature in accordance with other parameters is an effective way of achieving higher vapor flux in VMD with less energy (Li & Sirkar 2005). Figure 3 illustrates the resulting fluxes obtained, based on different flow rates. The insignificant increase in flux is related to the low increase in the Reynolds number. This influences the Nusselt number, the heat transfer coefficient, the vapor temperature, and finally, the saturation pressure of the feed solution. The increase in flow rate showed an intangible effect on flux which is in accordance with the modeled predictions. For example, doubling the flow raises flux by only about 6%. Hence, the effect of feed-water flow rate is minor when compared

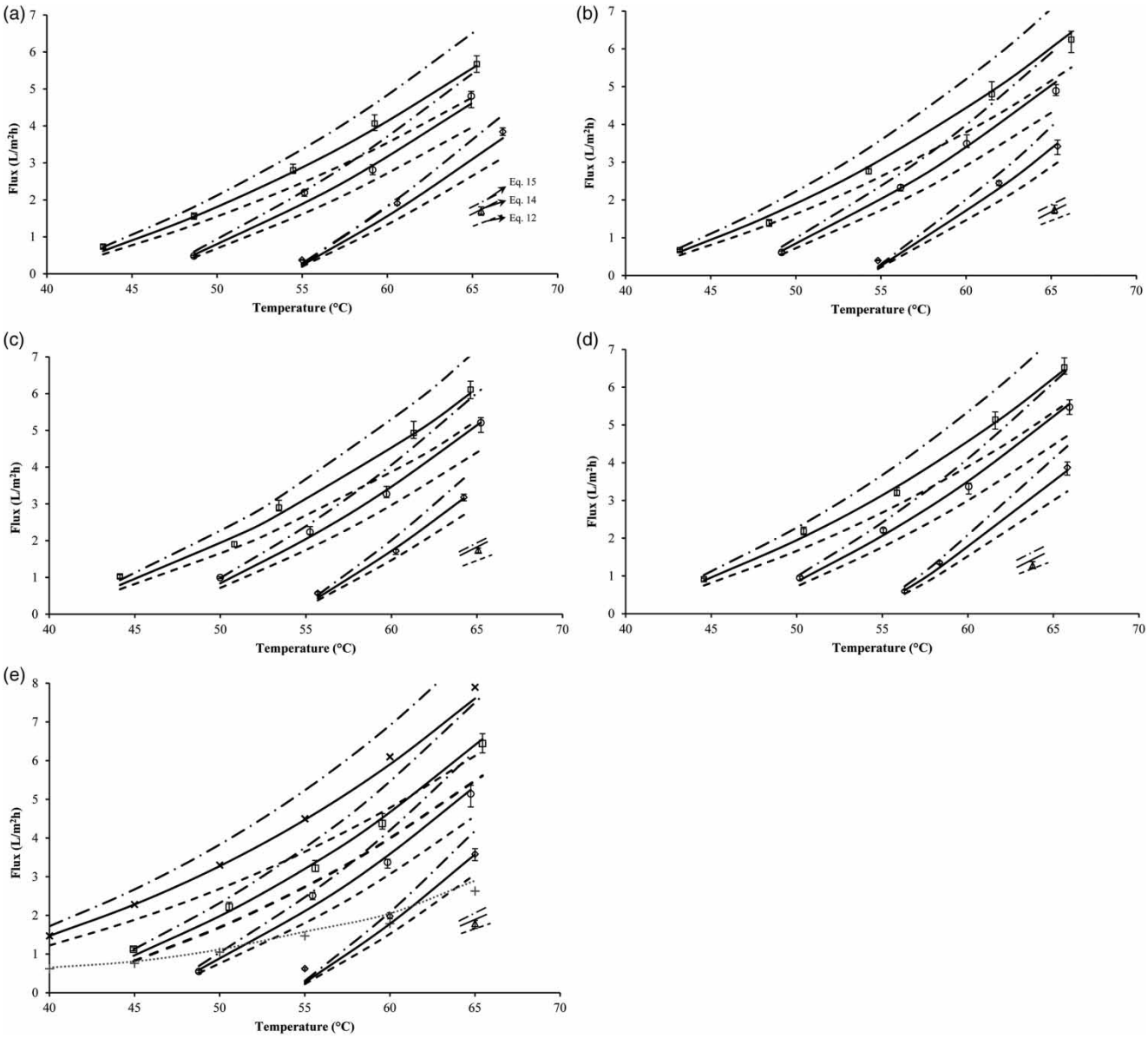

Figure 3 | Effects of pressure, temperature, and flow rate on permeate flux: (---) modeled flux (Equation (12)); (—) modeled flux (Equation (14)); (— • —) modeled flux (Equation (15)); (□) experimental flux ($P = 7$ kPa); (○) experimental flux ($P = 10$ kPa); (◇) experimental flux ($P = 15$ kPa); (Δ) experimental flux ($P = 20$ kPa); (x) experimental flux ($P = 3.5$ kPa) (Khayet & Matsuura 2011); (+) DCMD experimental flux ($T_p = 20$ °C) (Khayet & Matsuura 2011); (•••) DCMD modeled flux ($T_p = 20$ °C and flow rate = 4.88 L/min) (Khayet & Matsuura 2011) . (a) Flow rate = 0.5 L/min; (b) flow rate = 1 L/min; (c) flow rate = 1.5 L/min; (d) flow rate = 2 L/min; (e) flow rate = 6.90 L/min.

to bulk water temperature and vacuum pressure. The final set of experiments for turbulent flow (Re = 4,300) was implemented as presented in Figure 3(e). The results show that the experimental data agree well with the modeled permeate flux (Equation (14)). Experimental data from the literature using distilled water as a feed for VMD (Khayet & Matsuura 2011) are combined in Figure 3(e). The small difference between the experimental data and the model (Equation (14)) at high temperatures is due to the expansion of the membrane material. Equation (15) uses the smallest value for the membrane thickness, and this predicts higher values for permeate flux. The higher value for the Knudsen diffusion term also demonstrates this, especially at higher temperatures. In addition, experimental

and modeled data of a DCMD system (Khayet & Matsuura 2011) are incorporated to illustrate the strong effect of vacuum pressure in VMD especially at high temperatures.

Concentrations of 1, 2, 5, 10, 20, and 50 g/L saline solutions were obtained by mixing sodium chloride with distilled water. The effects of salinity concentration on permeate flux is shown in Figure 4. Feed-water temperature, flow rate, and permeate-side pressure were kept constant at 65 °C, 1 L/min, and 15 kPa, respectively. The most significant advantage of using VMD for desalination purposes is the negligible effect of salinity concentration on the rate of flux (Safavi & Mohammadi 2009). Figure 4 illustrates the small effect of feed-water salinity concentration on the permeate flux. The flux decline is imperceptible as estimated by the Knudsen–viscous diffusion models. The modeled flux was marginally above the experimental data by 4.76% and 12.33% for 1 and 50 g/L, respectively, as deposition of the dissolved solids on the membrane surface induced a lower rate of flux. The vapor pressure decreased slightly as salt concentration increased in VMD. The permeate flux rate declined as the NaCl concentration increased due to the influence of salt concentration on the activity coefficient (Wirth & Cabassud 2002). A comprehensive study of the scaling followed by developing a mathematical model for the decline rate of the permeate flux has been performed (Ramezanianpour *et al.* 2014). Over 99.9% of TDS removal was achieved by VMD, irrespective of feed-salt concentrations.

Specific energy consumption

The energy efficiency of the VMD process was investigated during the swimming pool salt-water treatment. The energy required for the vacuum pump, circulation pump, and water bath circulator was measured using a power meter for each test. Figure 5 shows the variation of specific energy consumption versus permeate flux, including and excluding heat energy. Since 1 kg permeate water was obtained in a shorter time at a higher flux rate, the specific energy consumption was reduced with increase in the flux. It was noted that the specific energy consumption reaches a relatively constant value at a high permeate flux rate when excluding heat energy (Sivakumar *et al.* 2013a). The specific energy consumption of VMD reduced as the flow rate increased. However, the variation was negligible compared to that with pressure and temperature fluctuations. The higher flux rate, due to lower absolute permeate-side pressure, decreases the energy consumption. However, a higher flux rate due to greater temperature increases the specific energy consumption. Therefore, it is suggested that VMD should be operated at a lowest absolute pressure while the heat energy is provided by another source of energy. Safavi & Mohammadi (2009) reported an energy consumption rate of 3.05, 2.29, and 1.67 kWh/kg for the VMD process with a flux of 9.6, 6.9, and 4.7 L/m^2.h, respectively, when operated at a permeate pressure of 10–12 kPa, with feed water set at 55 °C. These results are shown in Figure 5. The discrepancy between previous results and

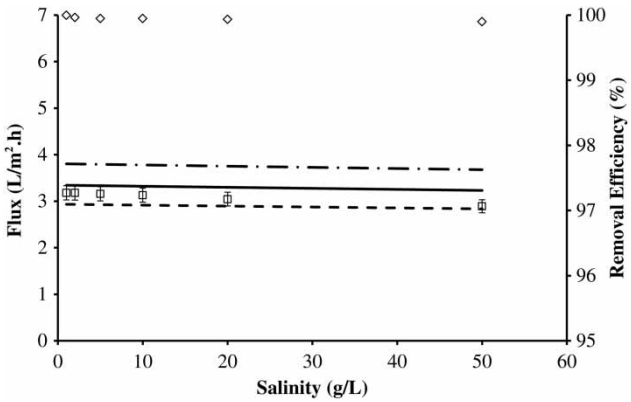

Figure 4 | Effects of feed-water salinity on flux: () modeled flux (Equation (13)); (—) modeled flux (Equation (14)); (— • —) modeled flux (Equation (15)); (□) experimental flux; (◇) removal efficiency. Temperature = 65 °C; vacuum pressure = 15 kPa; flow rate = 1 L/min.

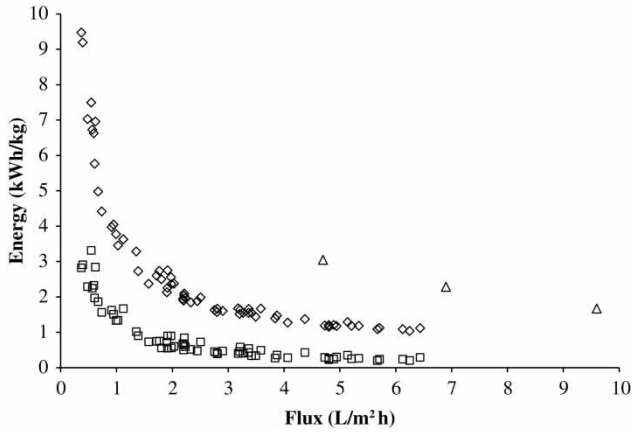

Figure 5 | Specific energy consumption of the VMD process versus permeate flux rate. (◇) Including heat; (□) excluding heat; (Δ) Safavi & Mohammadi (2009) data.

the results of this study is attributed to the difference in the membrane areas. A 4 cm^2 flat sheet membrane was used in the study presented. This means that the membrane area of the VMD process has to be larger in order to improve energy consumption (Cabassud & Wirth 2003).

Water quality analysis

The efficiency of VMD was investigated by the treatment of groundwater, seawater, mine-water effluent, and swimming pool salt water. The measurement of flux at various intervals shows that the initial flux was below the modeled clean water flux. The flux decreased 6.8%, 6.1%, 5.3%, and 5.8% over the duration of the experiment using groundwater, seawater, mine effluent water, and salt water, respectively. The flux decline is due to the deposition of suspended and dissolved solids on the membrane surface as a result of a high calcium concentration and particulate matter for groundwater and mine water, and high TDS concentration, especially sodium, in seawater and pool salt water.

Selected water quality parameters on raw feed water and the corresponding treated water are compared, based on the water quality guideline values in Table 1. It was generally found that the metals and TDS removal efficiency was as high as 99%. Standard total coliform tests using the membrane filter procedure were carried out on both feed water and permeate samples to determine microbial removal efficiency. No coliform was observed in the differently treated feed-water samples. Total coliform removal was expected, because it is well known that evaporation of feed water can remove total coliform. In all cases, the pH values dropped between the feed water and the permeate. This may be caused by the removal of alkalinity and the adsorption of atmospheric carbon dioxide in the permeate water. All permeate water quality values were sufficiently below the Australian Drinking Water Guideline (ADWG) and WHO guideline values.

A more detailed analysis of water quality parameters for swimming pool salt water is presented in Figure 6 for the 65 permeate samples. Figure 6(a) reveals that the TDS values plateau below 5.5 mg/L. The data are normally distributed for TOC concentration, and 89% of the values are between 0.15 and 0.5 mg/L, as shown in Figure 6(b). The average TOC concentration in the permeate was 0.325 mg/L. The distribution of TN data shows that 74% of the values are below 0.15 mg/L in an edge peak distribution graph. The distribution shape is due to the zero level of TN in 23% of the permeate samples. Figures 6(d)–6(f) illustrate that the distribution for Na, Mg, and Ca concentrations are skewed to the right. The

Table 1 | Water quality analysis

			Groundwater		Seawater		Mine effluent		Swimming pool water	
Parameter (mg/L)	ADWG	WHO	Feed	Permeate	Feed	Permeate	Feed	Permeate	Feed	Permeate
TDS	500	1,000	1,900	2.41	36,850	2.12	2,332	2.66	4,495	2.25
pH	6.5–8.5	6.5–9.2	7.52	6.15	7.98	6.15	7.68	6.32	7.28	6.38
Calcium	60–200	100–200	33.27	0.09	410	0.73	14.4	0.14	71.39	0.20
Magnesium	N/A	N/A	3.76	0.09	338	0.48	2.72	0.03	2.88	0.01
Sodium	200	180	6.82	0.15	10,700	0.73	15.37	0.08	2,420	0.43
Iron	0.3	0.2	8.69	0.07	0.32	0.00	1.92	0.04	N/A	N/A
Aluminum	0.2	0.2	0.67	0.00	0.18	0.00	3.38	0.00	N/A	N/A
Total coliforms	1	0	10	0.00	1,230	0.00	0.00	0.00	N/A	N/A
TOC	N/A	N/A	N/A	N/A	N/A	N/A	N/A	N/A	3.74	0.34
TN	N/A	N/A	N/A	N/A	N/A	N/A	N/A	N/A	6.09	0.09

All values in mg/L, except total coliforms which are measured in cfu/100 mL and pH.

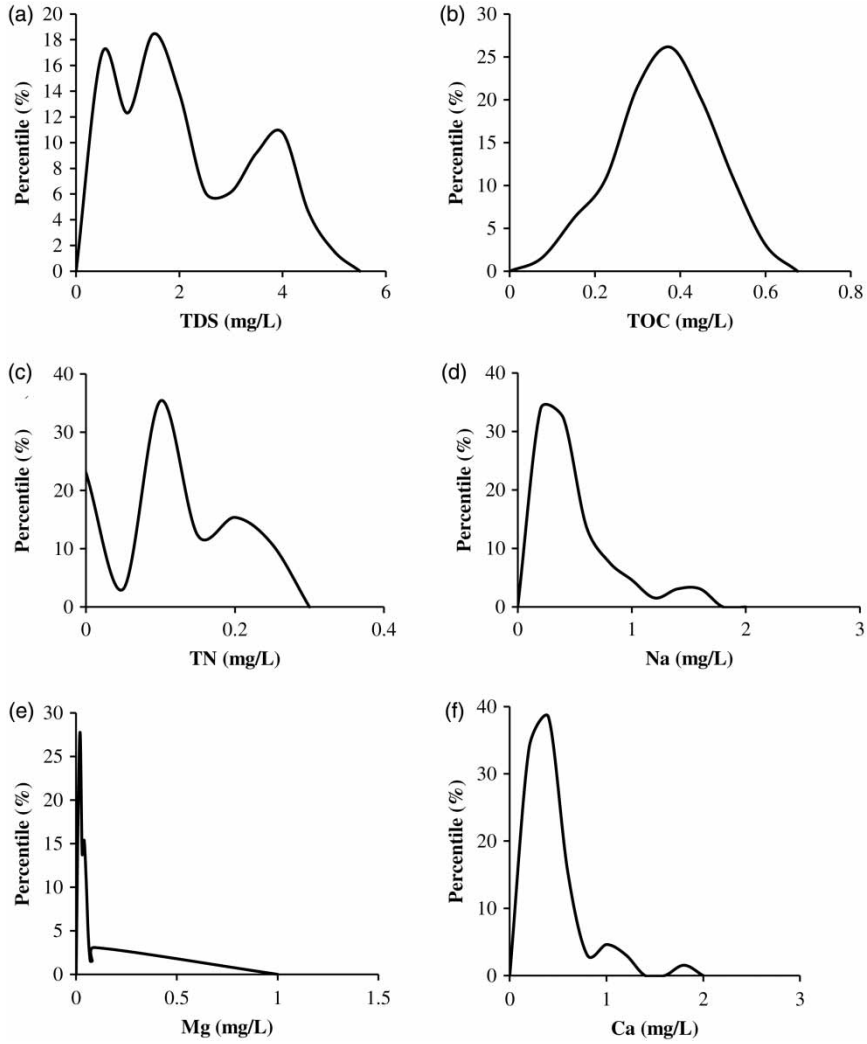

Figure 6 | Distribution of (a) TDS, (b) TOC, (c) TN, (d) Na, (e) Mg, and (f) Ca concentration of the permeate water from VMD.

concentration values for Na, Mg, and Ca are 92%, 89%, and 95% below 1, 0.05, and 1 mg/L, respectively. The skewed to the right distribution of Na, Mg, and Ca along with the edge peak distribution of TN illustrates the good performance of VMD in the treatment of brackish water samples. It can be noted that failure occurred in 2–10% of the tests. These results can be recognized in the TDS distribution graph, which implies that the peaks of the plateau distribution tend to the left. However, normal distribution of TOC concentrations in the permeate samples shows that organic carbon was produced, most likely because of the metabolic activities of living organisms or chemicals.

CONCLUSION

This study has shown that VMD can satisfactorily turn brackish water from four different sources into potable water. VMD was shown as an effective technology that has the potential to be as important as current pressure-driven membrane desalination because of its specific energy consumption. VMD processes can be carried out using a large membrane area, a requirement which is easy to meet.

Variation in the permeate flux was investigated under various operating conditions. Each of the parameters (feed-water temperature, salinity, flow rate, and vacuum

pressure) was varied independently and the corresponding flux rate recorded. These values were then compared to the theoretically predicted values for the same operating conditions. It was found that vacuum pressure was the most influential parameter, followed by feed-water temperature, flow rate, and finally salinity. A maximum flux rate of 6.44 L/m^2.h was achieved at a feed-water temperature of 65 °C, flow rate of 6.90 L/min, and pressure of 7 kPa on the permeate side.

The energy consumption of VMD was measured for each test. A higher flux rate due to a higher vacuum pressure was advantageous for increasing flux in an energy efficient manner. The specific energy consumption of the VMD process is directly related to the area of the membrane. It was concluded that a larger membrane area will reduce the specific energy consumption under the same operating conditions.

The VMD process was successfully implemented for desalinating and treating brackish water so that it could reach acceptable standards. The treatment capability of VMD is such that potable water can be produced from a variety of saline, brackish, and contaminated water sources. Contaminant removal efficiency remained considerably high for all contaminants and water sources. The average TDS, Ca, Mg, Na, Fe, Al, TOC, and TN removal efficiency was 99.9%, 99.6%, 99.0%, 99.3%, 99.0%, 100%, 90.9%, and 98.5%, respectively, and there was no observation of coliform in the permeate water samples. The parameters of pollutants measured in the permeate fell to within guideline values and this indicates that, although the treated water may require mineralization, permeate water is suitable for drinking.

REFERENCES

Al-Asheh, S., Banat, F., Qtaishat, M. & Al-Khateeb, M. 2006 Concentration of sucrose solutions via vacuum membrane distillation. *Desalination* **195** (1–3), 60–68.

Alkhudhiri, A., Darwish, N. & Hilal, N. 2012 Membrane distillation: a comprehensive review. *Desalination* **287**, 2–18.

Alklaibi, A. M. & Lior, N. 2005 Membrane-distillation desalination: status and potential. *Desalination* **171** (2), 111–131.

Al-Obaidani, S., Curcio, E., Macedonio, F., Di Profio, G., Al-Hinai, H. & Drioli, E. 2008 Potential of membrane distillation in seawater desalination: thermal efficiency, sensitivity study and cost estimation. *J. Membr. Sci.* **323** (1), 85–98.

Banat, F., Al-Rub, F. A. & Bani-Melhem, K. 2003 Desalination by vacuum membrane distillation: sensitivity analysis. *Sep. Purif. Technol.* **33** (1), 75–87.

Cabassud, C. & Wirth, D. 2003 Membrane distillation for water desalination: how to choose an appropriate membrane? *Desalination* **157** (1–3), 307–314.

Cerneaux, S., Strużyńska, I., Kujawski, W. M., Persin, M. & Larbot, A. 2009 Comparison of various membrane distillation methods for desalination using hydrophobic ceramic membranes. *J. Membr. Sci.* **337** (1–2), 55–60.

Chen, H., Wu, C., Jia, Y., Wang, X. & Lu, X. 2011 Comparison of three membrane distillation configurations and seawater desalination by vacuum membrane distillation. *Desalin. Water Treat.* **28** (1–3), 321–327.

Criscuoli, A., Carnevale, M. C. & Drioli, E. 2008 Evaluation of energy requirements in membrane distillation. *Chem. Eng. Process.* **47** (7), 1098–1105.

Guijt, C. M., Rácz, I. G., Reith, T. & de Haan, A. 2000 Determination of membrane properties for use in the modelling of a membrane distillation module. *Desalination* **132** (1–3), 255–261.

Jin, Z., Yang, D. L., Zhang, S. H. & Jian, X. G. 2008 Hydrophobic modification of poly(phthalazinone ether sulfone ketone) hollow fiber membrane for vacuum membrane distillation. *J. Membr. Sci.* **310** (1–2), 20–27.

Khayet, M. 2011 Membranes and theoretical modeling of membrane distillation: a review. *Adv. Colloid Interface Sci.* **164** (1–2), 56–88.

Khayet, M. & Matsuura, T. 2004 Pervaporation and vacuum membrane distillation processes: modeling and experiments. *AIChE J.* **50** (8), 1697–1712.

Khayet, M. & Matsuura, T. 2011 *Membrane Distillation: Principles and Applications.* Elsevier, The Netherlands.

Khayet, M., Velazquez, A. & Mengual, J. I. 2004 Modelling mass transport through a porous partition: effect of pore size distribution. *J. Non-Equil. Thermody.* **29** (3), 279–299.

Lawson, K. W. & Lloyd, D. R. 1996 Membrane distillation. I. Module design and performance evaluation using vacuum membrane distillation. *J. Membr. Sci.* **120** (1), 111–121.

Lawson, K. W. & Lloyd, D. R. 1997 Membrane distillation. *J. Membr. Sci.* **124**, 1–25.

Li, B. & Sirkar, K. K. 2005 Novel membrane and device for vacuum membrane distillation-based desalination process. *J. Membr. Sci.* **257** (1–2), 60–75.

Li, J.-M., Xu, Z.-K., Liu, Z.-M., Yuan, W.-F., Xiang, H., Wang, S.-Y. & Xu, Y.-Y. 2003 Microporous polypropylene and polyethylene hollow fiber membranes. Part 3. Experimental studies on membrane distillation for desalination. *Desalination* **155** (2), 153–156.

Mengual, J. I., Khayet, M. & Godino, M. P. 2004 Heat and mass transfer in vacuum membrane distillation. *Int. J. Heat Mass Transfer* **47** (4), 865–875.

Mericq, J.-P., Laborie, S. & Cabassud, C. 2010 Vacuum membrane distillation of seawater reverse osmosis brines. *Water Res*. **44** (18), 5260–5273.

Mericqa, J.-P., Laborieb, S. & Cabassud, C. 2011 Evaluation of systems coupling vacuum membrane distillation and solar energy for seawater desalination. *Chem. Eng. J*. **166**, 596–606.

Mohammadi, T. & Safavi, M. A. 2009 Application of Taguchi method in optimization of desalination by vacuum membrane distillation. *Desalination* **249** (1), 83–89.

Qtaishat, M., Matsuura, T., Kruczek, B. & Khayet, M. 2008 Heat and mass transfer analysis in direct contact membrane distillation. *Desalination* **219** (1–3), 272–292.

Ramezanianpour, M., Sivakumar, M. & Kruczek, B. 2014 An analytical flux decline model for membrane distillation. *Desalination* **345**, 1–12.

Safavi, M. & Mohammadi, T. 2009 High-salinity water desalination using VMD. *Chem. Eng. J*. **149** (1–3), 191–195.

Sivakumar, M., Ramezanianpour, M. & O'Halloran, G. 2013a Brackish water treatment for reuse using vacuum membrane distillation process. In: *9th IWA International Conference on Water Reuse*, 27–31 October 2013. Windhoek, Namibia, pp. 1–8.

Sivakumar, M., Ramezanianpour, M. & O'Halloran, G. 2013b Mine water treatment using a vacuum membrane distillation system. In: *4th International Conference on Environmental Science and Development*, Dubai, United Arab Emirates.

Wirth, D. & Cabassud, C. 2002 Water desalination using membrane distillation: comparison between inside/out and outside/in permeation. *Desalination* **147** (1–3), 139–145.

Xu, Y., Zhu, B.-K. & Xu, Y.-Y. 2006 Pilot test of vacuum membrane distillation for seawater desalination on a ship. *Desalination* **189** (1–3), 165–169.

Zhang, J., Li, J.-D., Duke, M., Hoang, M., Xie, Z., Groth, A., Tun, C. & Gray, S. 2013 Modelling of vacuum membrane distillation. *J. Membr. Sci*. **434**, 1–9.

First received 14 April 2014; accepted in revised form 3 October 2014. Available online 27 October 2014